Controlling particle properties in $YBa_2Cu_3O_{7-\delta}$ nanocomposites by combining PLD with an inert gas condensation system

M Sparing[1,4], E Reich[1,5], J Hänisch[1,2,4], T Gottschall[1,6], R Hühne[1], S Fähler[1], B Rellinghaus[1], L Schultz[1,3] and B Holzapfel[1,2]

[1] IFW Dresden, Institute for Metallic Materials, Helmholtzstrasse 20, D 01069 Dresden, Germany
[2] Karlsruhe Institute of Technology, Institute for Technical Physics, Hermann von Helmholtz Platz 1, D 76344 Eggenstein Leopoldshafen, Germany
[3] TU Dresden, Department of Mechanical Engineering, Institute for Materials Science, D 01062 Dresden, Germany

E mail: m.sparing@ifw dresden.de and jens.haenisch@kit.edu

Abstract

The critical current density J_c in $YBa_2Cu_3O_{7-\delta}$ thin films, which limits their application in external magnetic fields, can be enhanced by the introduction of artificial pinning centers such as non-superconducting nanoparticles inducing additional defects and local strain in the superconducting matrix. To understand the correlation between superconductivity, defect structures and particles, a controlled integration of particles with adjustable properties is essential. A powerful technique for the growth of isolated nanoparticles in the range of 10 nm is dc-magnetron sputtering in an inert gas flow. The inert gas condensation (IGC) of particles allows for an independent control of both the particle diameter distribution and the areal density. We report on the integration of such gas-phase-condensed HfO_2 nanoparticles into pulsed laser deposited (PLD) $YBa_2Cu_3O_{7-\delta}$ thin film multilayers with a combined PLD-IGC system. The particles and the structure of the multilayers are analyzed by transmission electron microscopy on cross-sectional FIB lamellae. As a result of the IGC particle implementation, randomly as well as biaxially oriented $BaHfO_3$ precipitates are formed in the $YBa_2Cu_3O_{7-\delta}$ thin films. With as few as three interlayers of nanoparticles, the pinning force density is enhanced in the low-field region.

Keywords: YBCO, thin films, $BaHfO_3$ (BHO), pinning, PLD, inert gas condensation

(Some figures may appear in colour only in the online journal)

1. Introduction

The application of $YBa_2Cu_3O_{7-\delta}$ (YBCO) based coated conductors in motors and generators requires, among others, high critical current densities J_c of the superconducting layer in external magnetic fields H. As J_c depends on the density and the character of pinning defects, many studies focus on the modification of the microstructure in order to enhance $J_c(H)$. One way to tailor the defect landscape of a superconductor is the implementation of artificial pinning centers via nanoparticles or precipitates. Although a variety of material systems and preparation routes have been used to introduce such particles [1 6], the correlation between particle properties, defect structure and superconducting properties

[4] Authors to whom any correspondence should be addressed.
[5] TU Dresden, ZIK BCube Center for Molecular Bioengineering, Arnoldstr. 18, D 01307 Dresden, Germany.
[6] Dresden High Magnetic Field Laboratory (HLD EMFL), Helmholtz Zentrum Dresden Rossendorf, Bautzner Landstraße 400, D 01328 Dresden, Germany.

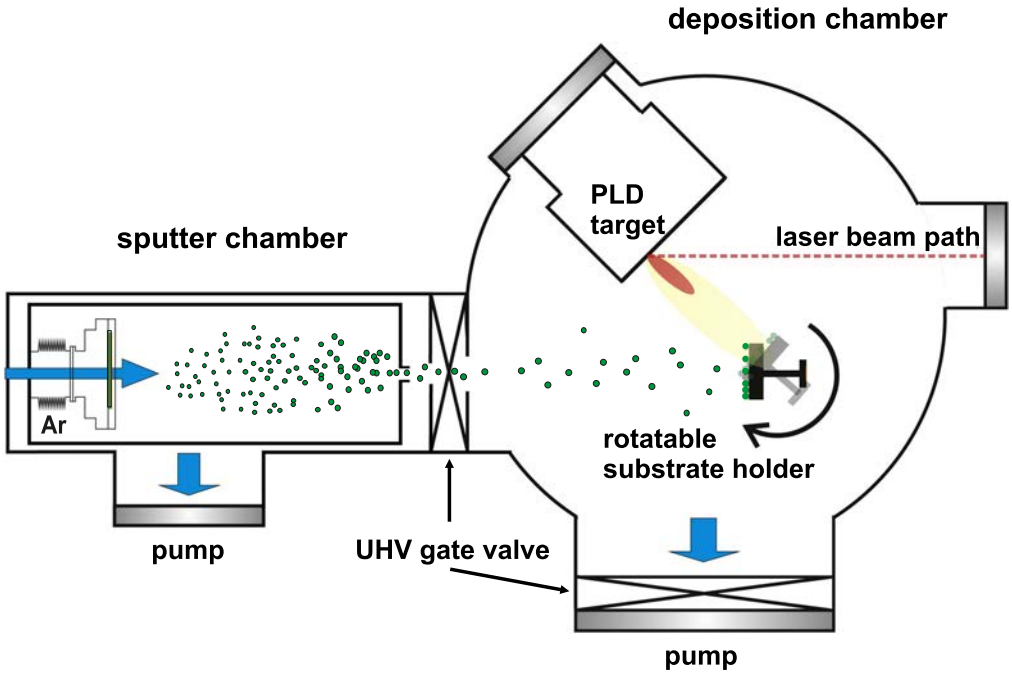

Figure 1. PLD IGC system combining a PLD setup with a magnetron sputtering device for inert gas condensation of nanoparticles (OAR *NC200U B*) in a single chamber. A system of gate valves and pumps allows for the growth of heterostructures by alternating thin film and particle deposition.

is still not fully understood [7]. This is mainly because a systematic, independent variation and control of the particle properties is rather difficult to achieve by pulsed laser deposition (PLD), metal-organic chemical vapor deposition or chemical solution deposition (CSD), the most common preparation methods for $YBa_2Cu_3O_{7-\delta}$ thin films.

A technique which allows for the preparation of isolated particles with a predefined diameter and an independently chosen areal density is the condensation of nanoparticles via DC-magnetron sputtering in an inert gas atmosphere, the so-called inert gas condensation process (IGC) [8, 9]. We already reported that $YBa_2Cu_3O_{7-\delta}$ thin films grown on substrates decorated with IGC particles show an improved $J_c(H)$ behavior [10]. The incorporation of such particles into $YBa_2Cu_3O_{7-\delta}$ thin films is the next step towards a systematic study of the particle influence on the pinning properties.

The preparation of nanocomposite films containing IGC nanoparticles, however, requires an experimental setup which combines a deposition technique for the $YBa_2Cu_3O_{7-\delta}$ matrix, in our case PLD, and a magnetron sputtering device for the particle preparation in a single chamber. Using $YBa_2Cu_3O_{7-\delta}$ thin films and HfO_2 nanoparticles, we show that combining these two processes is a technically feasible way to build up superconducting heterostructures with predefined IGC nanoparticles.

The experimental section of this paper gives a detailed description of our experimental setup, the architecture of our samples, and the preparation and analysis conditions. The results section consists of three parts. In section 3.1, the properties of HfO_2 particles grown by IGC are shown and their chemical nature is described. This is followed by an analysis of the structural properties of the nanocomposites in section 3.2; and in section 3.3, the improvement of the superconducting properties of heterostructures with IGC nanoparticles is shown in comparison to multilayers without particles.

2. Experimental details

2.1. Thin film and particle deposition

Superconducting heterostructures consisting of $YBa_2Cu_3O_{7-\delta}$ layers and incomplete interlayers of HfO_2 nanoparticles were prepared in our combined PLD-IGC system. This setup consists of a magnetron sputtering device for IGC of nanoparticles attached to a PLD chamber (figure 1). The growth of $YBa_2Cu_3O_{7-\delta}$ thin films requires an oxygen atmosphere in the range of $\approx$0.1 0.5 mbar, whereas the nanoparticles are deposited below $\approx 10^{-5}$ mbar. Consequently, the heterostructures have to be prepared by alternating between the two processes. A system of gate valves and pumps provides for a fast change between the different pressures and atmospheres. The preparation steps are described in the following paragraphs.

The $YBa_2Cu_3O_{7-\delta}$ thin films (and interlayers) were deposited in on-axis PLD geometry on (100) $SrTiO_3$ single crystal substrates. The material was ablated from a stoichiometric sintered target by means of a KrF excimer laser with a wavelength of 248 nm operated at a repetition rate of 5 Hz. The energy density at the target was around 1.7 J cm^{-2}. The substrates were glued to a heater with conductive silver paint and heated to 810 °C prior to deposition. This temperature was monitored with a thermocouple in the heating plate. The

Table 1. Geometrical and superconducting properties of the samples discussed in this paper. $n \times m$ YBCO layer number $\times$ YBCO laser pulses, L layer number, N areal density, d_P diameter, and v_P volume ratio of the particles.

$n \times m$	L	N μm^{-2}	d_P nm	v_P %	T_c K	H_{irr}(77 K) T	$f_{P\,max}$ GN m^{-3}
1×2000	0			0	91.8	8.5	2.9
4×500 400 °C	0			0	91.1	8.4	3.6
4×500 500 °C	0			0	91.1	8.4	3.9
4×500 400 °C	3	790	8	0.22	91.3	8.2	4.7
4×500 500 °C	3	1964	9	0.96	89.9	7.9	4.1
4×500 500 °C	3	2046	12	2.50	90.3	7.4	1.9

oxygen partial pressure during deposition was adjusted to 0.4 mbar. With our chamber geometry, this results in a $YBa_2Cu_3O_{7-\delta}$ growth rate of about 1.2 Å/pulse.

A cluster gun (OAR *NC200U-B*) was used to prepare the nanoparticles. In the inert gas phase condensation process, a supersaturated metal vapor is generated from a metallic hafnium target by DC-magnetron sputtering. Nanoparticles nucleate and grow in an Ar atmosphere of 0.5 mbar and are subsequently ejected into high vacuum (10^{-5} mbar) via differential pumping. The mean particle size can be controlled by varying the sputtering power, the gas pressure, and/or the gas mixture. The areal density of the nanoparticles is adjusted by the deposition time.

During the particle deposition, the $YBa_2Cu_3O_{7-\delta}$ layers are repeatedly exposed to a pressure below 10^{-2} mbar for several minutes. At the $YBa_2Cu_3O_{7-\delta}$ deposition temperature of 810 °C, this would lead to a phase degradation of the $YBa_2Cu_3O_{7-\delta}$ [11] and a depletion of oxygen [12, 13]. To prevent this degradation, the multilayer samples and their respective references were cooled to 500 °C or 400 °C in 400 mbar oxygen with 20 K min^{-1} prior to the deposition of each particle interlayer. After each particle deposition, the samples were heated again to 810 °C in 0.4 mbar O_2 prior to the deposition of the next $YBa_2Cu_3O_{7-\delta}$ layer. Following the deposition of the last $YBa_2Cu_3O_{7-\delta}$ layer, the films were cooled with 10 K min^{-1} in 400 mbar O_2 to realize optimum oxygen loading.

2.2. Architecture of the $YBa_2Cu_3O_{7-\delta}$–HfO_2 nanoparticle heterostructures

Heterostructures of four $YBa_2Cu_3O_{7-\delta}$ layers (each 500 pulses) and three particle interlayers (see figure 7) were grown as described above. The particle volume content v_P

$$v_P = \frac{\pi {d_P}^3}{6} \cdot \frac{N \cdot L}{t}, \qquad (1)$$

i.e. the ratio between the volume of all particles incorporated into the heterostructure and the volume of the thin film, where L is the number of particle interlayers and t the total film thickness, was controlled by independently varying diameter d_P and areal density N of the HfO_2 particles. Table 1 gives an overview of the samples discussed in this paper. The respective reference samples were prepared under exactly the same conditions as the corresponding multilayers with particles including the changes of temperature and atmosphere in between the deposition of the $YBa_2Cu_3O_{7-\delta}$ layers. This enables us to distinguish between effects arising solely from the stacking of the $YBa_2Cu_3O_{7-\delta}$ layers and the additional influence of the particles.

2.3. Characterization

Morphology and size of the nanoparticles were analyzed by transmission electron microscopy (TEM) (FEI Tecnai T20, 200 kV) using particles deposited on conventional carbon-coated copper TEM grids. These reference samples were deposited under the same conditions as the particles on the substrates [10]. The distribution of the particle diameter was determined from an ensemble of over 200 particles per sample. For this purpose, the long and short half-axis of each particle was measured and the volume calculated using the shorter length as the particle height. The particle diameter was defined by the corresponding equivolume spherical particle. The areal density N was measured by counting the particles on a sample area of at least 1 μm^2. The electron energy loss spectra and the high-resolution TEM images of the particles where taken at an *FEI* Titan^3 operated at 300 kV.

The structural properties of the films were studied using x-ray diffraction in θ-2θ geometry (Co-K_α) and a texture goniometer (Cu-K_α) for pole figure measurements. The thin film topography was investigated with a scanning electron microscope (SEM) Philips XL 20 at 20 kV. The particles in the YBCO multilayers were imaged by TEM (FEI Tecnai T20, 200 kV) on cross-sectional lamellae prepared in a dual beam focused ion beam system *FEI Helios Nanolab 600i*. The local element distribution was analyzed by scanning TEM (STEM) in combination with energy dispersive x-ray spectroscopy (EDX).

The transition temperature T_c, the transport critical current density J_c and the corresponding pinning force F_p were determined on bridges of 50 μm width and 0.8 mm length. These bridges were photolithographically patterned and structured by Ar^+ ion etching. Electrical transport properties were studied at 77 K in magnetic fields up to 9 T using a standard four-probe geometry in a Quantum Design PPMS. The critical current density J_c was defined with an electrical-field criterion of 1 μV cm^{-1}. The irreversibility field H_{irr} has been defined with an electrical-field criterion of 10 μV cm^{-1} from $R(T)$ measurements ($I_{meas} = 100\ \mu$A, $J = 800$ A cm^{-2}) at constant magnetic fields.

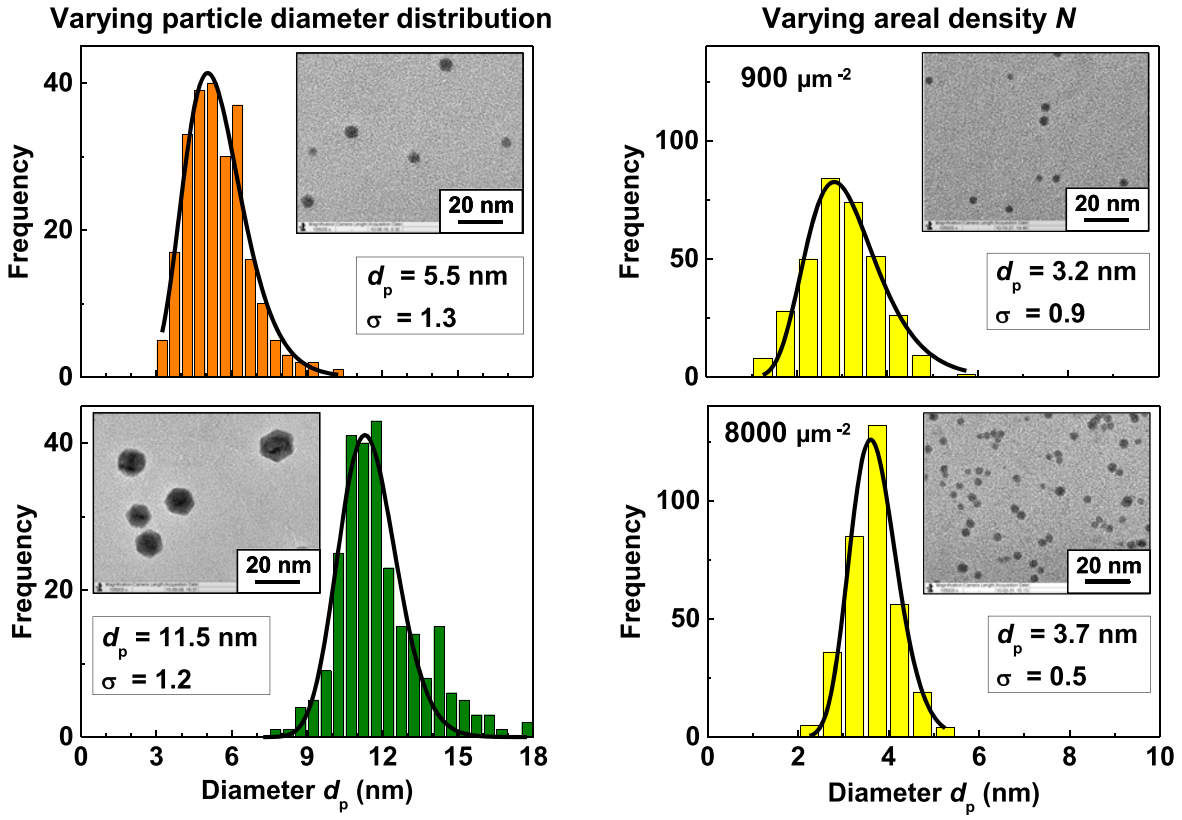

Figure 2. The particle diameter distribution (left side) and the mean particle diameter d_P are regulated by the sputtering parameters, the areal density N (right side) depends on the deposition time. The size distribution for HfO_2 particles follows a log normal function [14]. The particles are isolated and randomly distributed all over the sample.

3. Results and discussion

3.1. IGC nanoparticles

Nanoparticles with a mean diameter between 3 nm and 12 nm were grown from a hafnium target via DC magnetron sputtering in Ar atmosphere. The particle preparation conditions were chosen in such a way that isolated particles of a predefined diameter are distributed randomly all over the sample. As an example, we show the analysis of TEM pictures of several samples of HfO_2 nanoparticles on amorphous carbon (figure 2). For all mean particle diameters we observe a very narrow size distribution, which can be fitted by a log-normal function [14]. More than 70% of the particles on each sample are isolated and less than 7% are found in agglomerates of three or more particles.

The calculation of the hafnium content in the heterostructures is based on the measurement of the particle size on the TEM-grid references. Therefore, it is crucial to know whether the nature of these particles is purely metallic, oxidic or a combination of both. Although the particles were grown from a metallic hafnium target in an inert gas atmosphere, they can oxidize to HfO_2 either through residual oxygen or after they are taken out of the deposition chamber.

For two reasons, we conclude that the particles are fully oxygenated: first, they exhibit a uniform contrast in the TEM pictures (figure 3(a)) without indication of a core shell structure. The oxidic nature is confirmed by lattice parameters of the particles, which were calculated from the intensity maxima in the Fourier transformation of the image (figure 3(a) right). These maxima correspond to Bragg reflexes in the diffraction image. The three inner reflexes originate from lattice planes with a distance $d \geqslant 2.94$ Å ($1/d \leqslant 3.4$ nm^{-1}). This indicates an oxygenation of the particle, as the biggest lattice constant in pure hafnium in the hexagonal modification is $d_{100} = 2.768$ Å ($1/d = 3.61$ nm ^{1}) [15]. The reflex with $1/d = 2.72$ nm ^{1} ($d = 3.67$ Å) corresponds to the (110) reflex of monoclinic HfO_2 [15]. The two other inner reflexes can be attributed to HfO_2 ($\bar{1}11$) and (111).

A second indication for the oxidation of the particles is given by an electron energy loss spectroscopy (EELS) line scan over two neighboring particles (figures 3(b) (d)). The intensity of the oxygen K-edge (energy = 532 eV) is enhanced at the site of the particles and decreases significantly between the particles (figure 3(d)).

3.2. Structural properties of the heterostructures

The c-axis oriented growth of $YBa_2Cu_3O_{7-\delta}$ on $SrTiO_3$ is verified by the (00l) diffraction peaks of $YBa_2Cu_3O_{7-\delta}$ in the XRD θ-2θ scan for both a (1 × 2000) thin film and the (4 × 500) multilayers with $BaHfO_3$ particles (figure 4). Additionally, Y_2O_3 and $BaHfO_3$ are identified as secondary phases. The change of the atmosphere in the deposition chamber for particle deposition in between the $YBa_2Cu_3O_{7-\delta}$

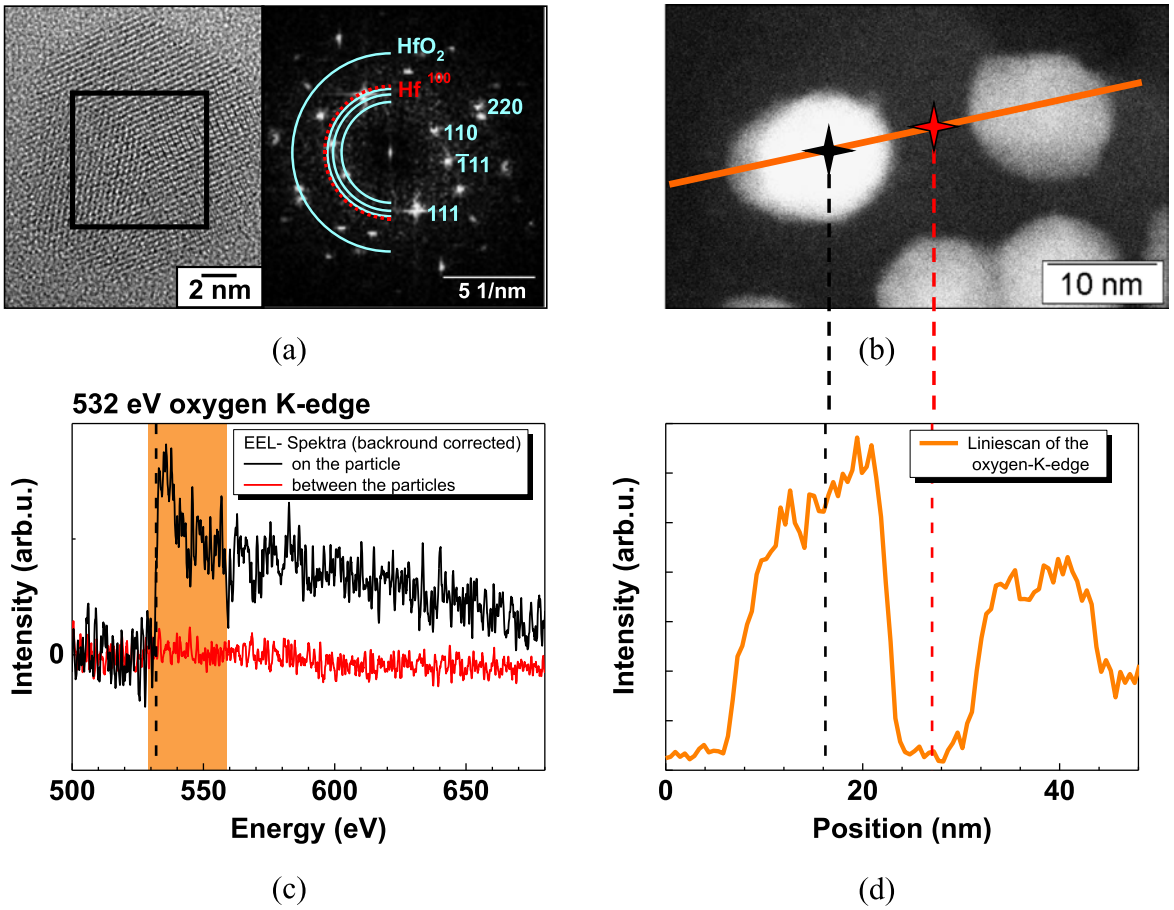

Figure 3. Oxidation of a nanoparticle grown by IGC from a hafnium target: (a) high resolution TEM image of a HfO_2 nanoparticle. In the Fourier transformation (right), reflexes of HfO_2 are clearly identified. (b) High angle annular dark field (HAADF) image of the scanning transmission electron microscopic (STEM) analysis of two HfO_2 particles. (c) Electron energy loss spectra in the energy window of the oxygen K edge on the site of a particle (blue) and in between particles (red). (d) Line scan of the oxygen K edge over two particles. The intensity of the oxygen K edge (energy = 532 eV) is enhanced at the particles.

layers is not promoting the formation of cuprate phases other than $YBa_2Cu_3O_{7-\delta}$ in the films.

The incorporation of hafnium(oxide) nanoparticles in $YBa_2Cu_3O_{7-\delta}$ leads to the formation of $BaHfO_3$ in the heterostructures (figure 4), similar to previous works on $YBa_2Cu_3O_{7-\delta}$/Hf quasi-multilayers [3, 16]. The amount of $BaHfO_3$ in the samples augments with increasing HfO_2 particle content as indicated by the higher $BaHfO_3$ (400) peak, which originates from biaxially textured $BaHfO_3$ particles in the $YBa_2Cu_3O_{7-\delta}$ matrix. A HfO_2 particle volume content of $v_P = 1\%$ corresponds to a content of 4.8 mol% HfO_2 in the $YBa_2Cu_3O_{7-\delta}$ thin film. Assuming a complete reaction to $BaHfO_3$, this results in 2 vol% $BaHfO_3$ in the $YBa_2Cu_3O_{7-\delta}$ multilayer.

With rising hafnium content, the Y_2O_3 (400) peak decreases, which suggests an influence of the hafnium particles on the Y_2O_3 formation. This strong anti-correlation between Y_2O_3 and $BaHfO_3$ peaks has recently also been observed in CSD- [18] as well as PLD-grown nanocomposites [19] and indicates a partial incorporation of Y in $BaHfO_3$.

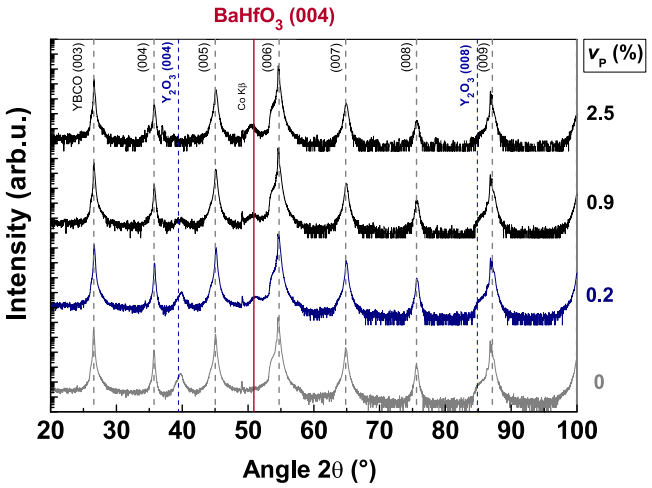

Figure 4. XRD θ 2θ scans of three 4 × 500 $YBa_2Cu_3O_{7-\delta}$ nanoparticle heterostructures compared to a reference $YBa_2Cu_3O_{7-\delta}$ (1 × 2000) film with a thickness of 240 nm. The HfO_2 particles react with $YBa_2Cu_3O_{7-\delta}$ to $BaHfO_3$. The intensity of the $BaHfO_3$ (004) peak increases and the Y_2O_3 (004) peak decreases with HfO_2 particle volume content v_P.

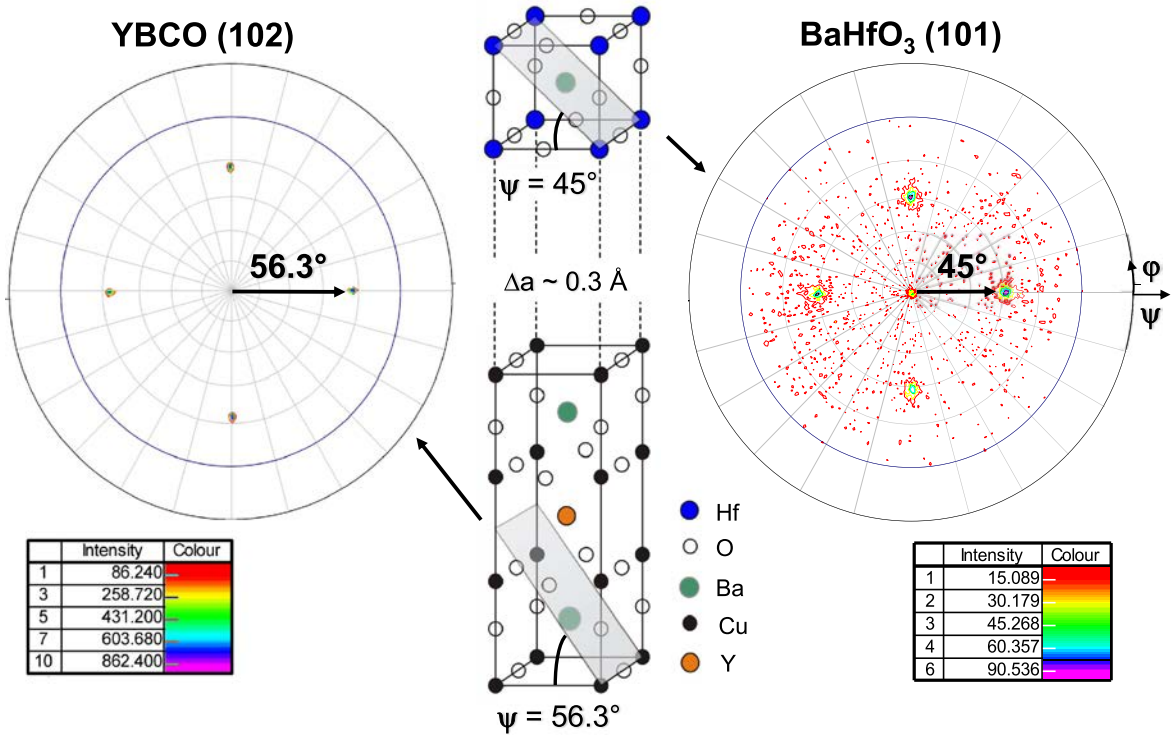

Figure 5. Pole figures of $YBa_2Cu_3O_{7-\delta}$ (102) and $BaHfO_3$ (101) of a multilayer with a particle content of $v_P = 2.5$ vol%. A fraction of the $BaHfO_3$ grows cube on cube to $YBa_2Cu_3O_{7-\delta}(001)[100]_{BaHfO_3}||(001)[100]_{YBCO}$. The small additional peak in the center of the $BaHfO_3$ pole figure arises from $YBa_2Cu_3O_{7-\delta}$ (004), which overlaps with $BaHfO_3$ (101).

A large fraction of the $BaHfO_3$ particles grows *c*-axis-oriented with a texture relation of $(001)[100]_{BaHfO_3}||(001)[100]_{YBCO}$ as shown in the pole figures of the $v_P = 2.5\%$ sample (figure 5). This so-called cube-on-cube texture relation was also found in on- and off-axis deposited $YBa_2Cu_3O_{7-\delta}$/Hf quasi-multilayers [3, 16], where the $BaHfO_3$ particles grow on the YBCO surface directly. The fraction of textured particles in the matrix, however, cannot be quantified on the basis of the available diffraction data. A rough estimate based on TEM images on cross-sectional FIB lamellae indicates between 40% and 60% of textured particles. This is comparable to CSD-grown nanocomposites with small densities of single perovskite nanoparticles [17] in contrast to nearly 100% in PLD-grown films. The randomly oriented arrival of the HfO_2 particles at the surface would result in a much smaller textured fraction than observed. Consequently, some HfO_2 particles reorient upon arrival and/or during film growth and $BaHfO_3$ formation.

The individual particles react with the surrounding $YBa_2Cu_3O_{7-\delta}$ to spherical $BaHfO_3$ and remain in the layers in which they were incorporated into the film. As the TEM and STEM-EDX images (figures 6 and 7) illustrate, there is no interlayer correlation between the particles. Figure 6 shows TEM and corresponding diffraction patterns of the cross-section FIB lamella of a (5×500) $YBa_2Cu_3O_{7-\delta}$ multilayer with a particle content of $v_P = 0.2\%$. The individual particles are identified through the Moiré contrast between the $BaHfO_3$ and the $YBa_2Cu_3O_{7-\delta}$ lattice. The measured Moiré fringe distance of 3.4 nm is of the order of the calculated interference between the $(00l)$ lattices of $YBa_2Cu_3O_{7-\delta}$ and $BaHfO_3$ $(1/\Delta g = d_{(006)YBCO}/(1 - d_{(004)BaHfO_3}/d_{(006)YBCO}) =$ 3.2 nm, [20]). The particles are located in the three equidistant layers ($\Delta = 60$ nm) as deposited. The diameter of the individual particles measured from the TEM images is slightly bigger than the initial particle size. Taking into account the expected volume increase of 28% during the reaction of HfO_2 to $BaHfO_3$ and the lack of statistics in this image, we conclude that the majority of the particles does not agglomerate in the interlayer. This is different from quasi-multilayers with PLD-grown $BaHfO_3$ or $BaZrO_3$ particles, where round and/or columnar nanostructures may form across several $YBa_2Cu_3O_{7-\delta}$ interlayers for small interlayer distances [21, 22]. The EDX map of the hafnium distribution in a cross-section FIB lamella of a multilayer with 2.5 vol% is an additional confirmation that hafnium is found primarily in between the $YBa_2Cu_3O_{7-\delta}$ layers (figure 7).

The topography of $YBa_2Cu_3O_{7-\delta}$ thin films with HfO_2 particles deposited on the substrate or in between layers is different from $YBa_2Cu_3O_{7-\delta}$ thin films or multilayers without particles. Figure 8 shows the SEM image of two $YBa_2Cu_3O_{7-\delta}$ thin films with particles deposited only on one half of the sample (samples not listed in table 1). The side with particles has a higher density of large holes and a different hole geometry, it also appears brighter. We did not observe pores protruding all the way down to the substrate in TEM images. Therefore, we conclude that the pores extend only in a small range at the surface over several few unit cells. The reason behind this effect is most likely an influence of the

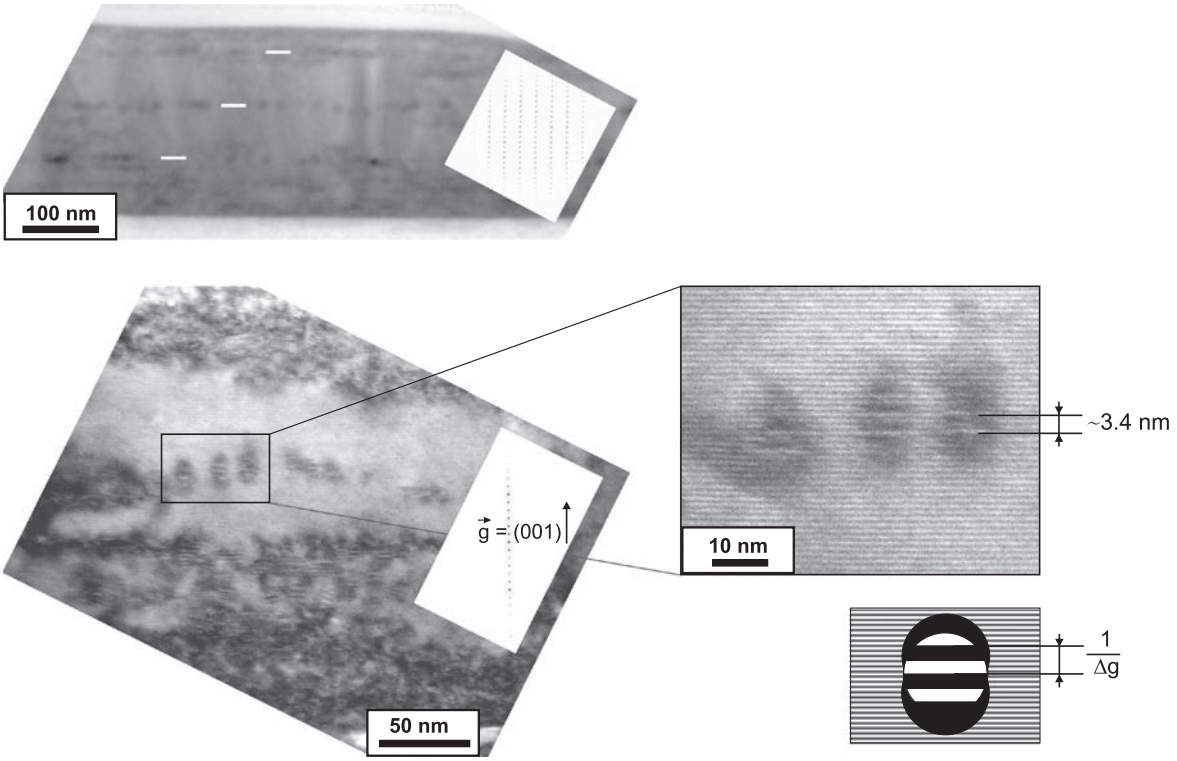

Figure 6. TEM and corresponding diffraction patterns of the cross section FIB lamella of a (5 × 500) YBCO multilayer with a particle content of 0.2 vol%. The particles are located in three equidistant layers (highlighted with white lines in the upper image) in which they were deposited. The individual particles are identified through the Moiré contrast between the lattices of $BaHfO_3$ and $YBa_2Cu_3O_{7-\delta}$.

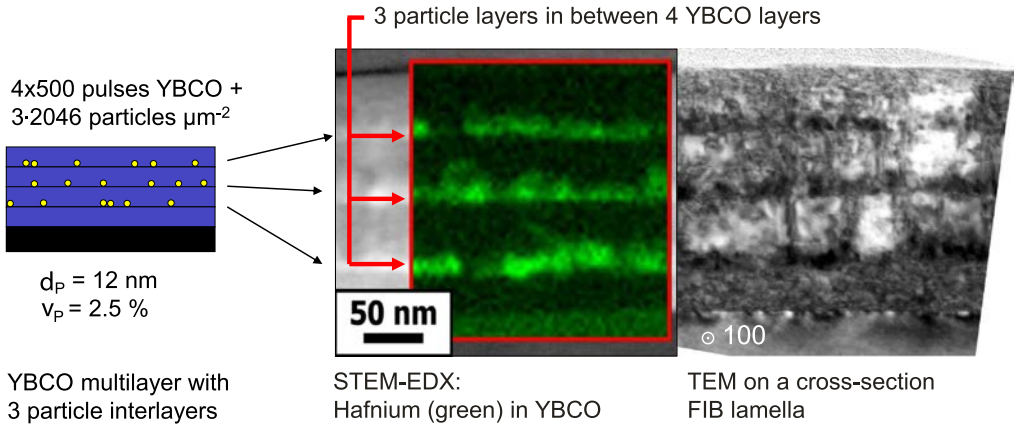

Figure 7. The YBCO $BaHfO_3$ nanocomposites are built up by 4 × 500 pulses of $YBa_2Cu_3O_{7-\delta}$ + 3 HfO_2 nanoparticle interlayers with predefined areal density N and particle diameter d_P. The cross sectional hafnium EDX map of a multilayer with 2.5 vol% shows the hafnium being primarily located in between the $YBa_2Cu_3O_{7-\delta}$ layers.

particles on the nucleation and growth of $YBa_2Cu_3O_{7-\delta}$ (trend towards stronger island growth with particle insertion). A similar increase in pore density (however with reducing pore diameter) has been observed in 211/YBCO quasi-multilayers on 10° vicinal substrates and was explained there by strain effects [23]. To which extend the superconducting properties of multilayers with particles are influenced by this increased porosity cannot be clarified, as the effect is not separable from the particle influence itself. The increased porosity might, e.g., lead to a faster oxygenation in multilayers with particles.

3.3. Superconducting properties of the heterostructures

The influence of the multilayer growth and the $BaHfO_3$ particles on the electrical properties of $YBa_2Cu_3O_{7-\delta}$ thin films is discussed on the basis of the pinning force density f_P versus the reduced magnetic field $h = H/H_{irr}$ in figure 9. The

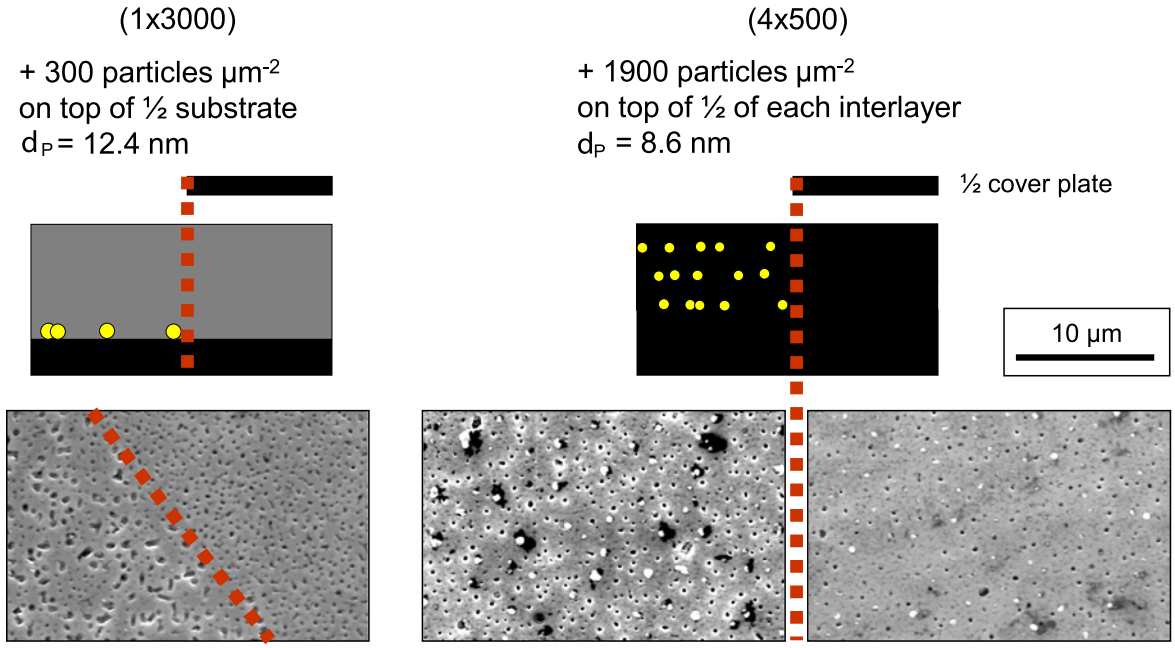

Figure 8. The particles influence the film morphology. The SEM images of $YBa_2Cu_3O_{7-\delta}$ surfaces with particles on the substrate (left) or in between the $YBa_2Cu_3O_{7-\delta}$ layers (right) show more holes and a different hole geometry compared to the respective particle free sample side.

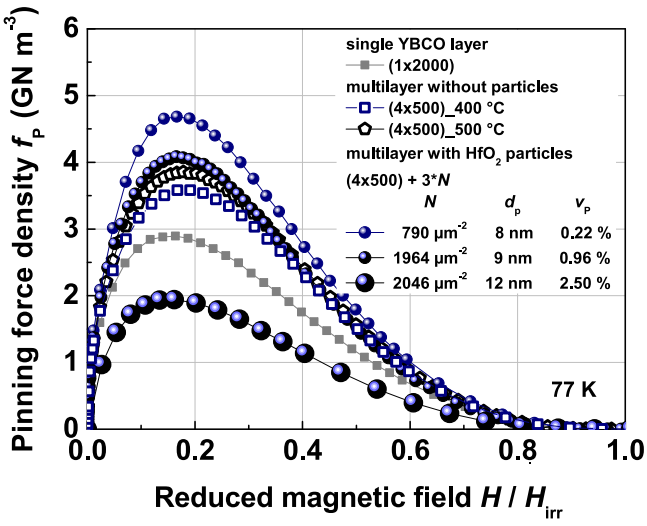

Figure 9. Pinning force density f_P versus reduced magnetic field $h = H/H_{irr}$ for $H \| c$ at 77 K. In the two multilayers with HfO_2 particles with $v_P \leqslant 1$ vol% f_P is enhanced compared to the $YBa_2Cu_3O_{7-\delta}$ thin films without particles.

respective critical temperatures and irreversibility field values are given in table 1.

The 4 × 500 multilayers *without* particles have a higher f_P than the 1 × 2000 reference thin film, in spite of their lower T_c. This indicates that the special growth conditions for PLD-IGC heterostructures described in section 2.1 (i.e. repeated atmospheric changes as well as heating and cooling cycles during the multilayer growth) influence the microstructure and thereby the electrical properties of the multilayers. As a consequence, the influence of the particles or individual particle properties on the structural and electrical properties of $YBa_2Cu_3O_{7-\delta}$ can only be assessed correctly in comparison to a particle-free multilayer with the same growth profile. The multilayers *with* particles show different f_P curves compared to the reference multilayers without particles. In the two multilayers with a particle volume content $v_P \leqslant 1\%$ and comparable particle diameters ($d_P = 8$ and 9 nm) f_P is increased, whereas f_P of the multilayers with $v_P = 2.5\%$ ($d_P = 12$ nm) is considerably reduced. The largest maximum of the pinning force density f_{Pmax} of 4.8 GN m^{-3} at 77 K is observed in the multilayer with the smallest number of particles per layer ($N = 790\,\mu m^{-2}$). Hence, an increase in the particle density does not necessarily lead to an effective enhancement of the pinning force density in our films. This could be a consequence of the corresponding increase in particle volume content v_P as well as areal density N. A high particle volume content or rather a high surface coverage with particles $A_P = N \cdot d_P$ can lead to an increased defect density and local disturbances of the epitaxy between the $YBa_2Cu_3O_{7-\delta}$ interlayers, which reduces the superconducting cross-section. This can be illustrated by a simple example: for an areal density of $N = 2050$ particles µm^{-2}, the average distance between two particle centers is around 24 nm. In combination with a particle diameter of $d_P \geqslant 12$ nm, the distance between two particles is of the order of the particle diameter, the surface coverage $A_P \approx 25\%$ and a disturbed growth of the YBCO matrix likely. Furthermore, the formation of unfavorably large pores, acting as current blockers, might be enhanced for larger areal particle densities, similar to larger Y_2O_3 precipitates [25].

Samples with and without $BaHfO_3$ particles show a similar anisotropy of J_c with respect to magnetic field orientation. Figure 10 compares the angular dependence of J_c of the multilayer with the highest $f_{Pmax} = 4.8$ GN m^{-3} ($v_P = 0.22\%$) and its reference multilayer without particles at 77 K for two magnetic

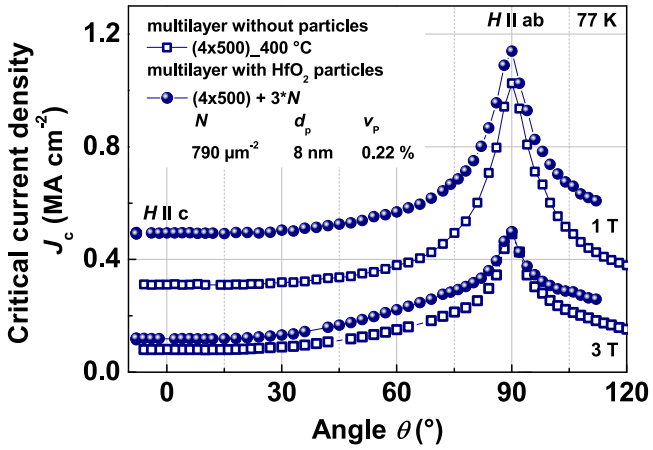

Figure 10. J_c anisotropy of a multilayer with HfO_2 particles ($v_P = 0.22$ vol%) compared to the reference $YBa_2Cu_3O_{7-\delta}$ multi layer without particles at 77 K for two magnetic fields. J_c is enhanced by the nanoparticles in a wide angular range around $H\|c$.

fields. Both thin films show the usual J_c maximum for $H\|ab$ ($\theta = 90°$). This J_c maximum at $H\|ab$ results from two contributions. A broad maximum governed by the mass anisotropy of $YBa_2Cu_3O_{7-\delta}$ and randomly distributed isotropic defects, and a sharper maximum due to pinning on extended planar defects [24]. A similar *ab*-peak height in both films points to a comparable density of planar defects such as stacking faults. The addition of nanoparticles leads predominantly to an increase in J_c in a wide angular range around $H\|c$. The enhancement of J_c is very similar to CSD-grown films with *in-situ* $BaZrO_3$ [26] and $BaHfO_3$ [18] as well as preformed $BaZrO_3$ [27] nanoparticles. This is due to the large distances between the particles, the absence of *c*-axis correlations between them or even the formation of nanocolumns and the similar fraction of randomly oriented nanoparticles. Although this increase of J_c is moderate, it was obtained with only three interlayers of nanoparticles and may be further enhanced by increasing the number of particle interlayers, i.e. reducing the interlayer distance.

4. Conclusion

Superconducting heterostructures of predefined IGC nanoparticles and thin film multilayers were grown in a novel PLD-IGC system. This highly flexible technique allows for a unique control of the particle properties such as material, areal density, and diameter of the particles as well as the number of interlayers independently of each other. The special growth conditions for PLD-IGC heterostructures (repeated atmospheric changes as well as heating and cooling cycles during the multilayer growth) influence the microstructure and therewith the electrical properties of the multilayer. Therefore, the influence of the particles on the structural and electrical properties of $YBa_2Cu_3O_{7-\delta}$ has to be assessed in comparison to a particle-free multilayer with the same growth profile. The example of HfO_2 nanoparticle interlayers in $YBa_2Cu_3O_{7-\delta}$ thin films shows that cube-on-cube-textured as well as randomly oriented $BaHfO_3$ precipitates are formed in the $YBa_2Cu_3O_{7-\delta}$ thin films as a result of the IGC particle implementation. With as few as three interlayers of nanoparticles, the pinning force density could be enhanced in fields around 1 T in a wide angular range around $H\|c$.

Acknowledgments

The authors thank Ralf Voigtländer, Alexander Horst, Uwe Reinhold, Peter Werner, Steffen Grundkowski, Jürgen Möhler, F Thunig, and Tina Sturm for their assistance with the construction of the experimental setup, Ingo Mönch for photolithography, Yiliang Xu for programming the motor control, Elias Mohn for fruitful discussions as well as Darius Pohl and Anja Bonatto Minella for EELS measurements and high-resolution TEM images. The work and results reported in this publication were partially funded by the EU-FP6 research project *Nanoengineered Superconductors for Power Applications* NESPA no. MRTN-CT-2006-035619 and the *Studienstiftung des deutschen Volkes*.

References

[1] Obradors X, Puig T, Palau A, Pomar A, Sandiumenge F, Mele P and Matsumoto K 2011 3.10 Nanostructured superconductors with efficient vortex pinning *Comprehensive Nanoscience and Technology* ed D L Andrews, G D Scholes and G P Wiederrecht (Amsterdam: Academic) pp 303 49

[2] Gapud A A, Kumar D, Viswanathan S K, Cantoni C, Varela M, Abiade J, Pennycook S J and Christen D K 2005 Enhancement of flux pinning in $YBa_2Cu_3O_{7-\delta}$ thin films embedded with epitaxially grown Y_2O_3 nanostructures using a multi layering process *Supercond. Sci. Technol.* **18** 1502

[3] Hänisch J, Cai C, Stehr V, Hühne R, Lyubina J, Nenkov K, Fuchs G, Schultz L and Holzapfel B 2006 Formation and pinning properties of growth controlled nanoscale precipitates in $YBa_2Cu_3O_{7-\delta}$ transition metal quasi multilayers *Supercond. Sci. Technol.* **19** 534

[4] Mele P, Matsumoto K, Ichinose A, Mukaida M, Yoshida Y, Horii S and Kita R 2008 Systematic study of the $BaSnO_3$ insertion effect on the properties of $YBa_2Cu_3O_{7-\delta}$ films prepared by pulsed laser ablation *Supercond. Sci. Technol.* **21** 125017

[5] Reich E, Thersleff T, Hühne R, Iida K, Schultz L and Holzapfel B 2009 Structural and pinning properties of $Y_2Ba_4CuMO_y$ (M = Nb, Zr)/$YBa_2Cu_3O_{7-\delta}$ quasi multilayers fabricated by off axis pulsed laser deposition *Supercond. Sci. Technol.* **22** 105004

[6] Harrington S A, Durrell J H, Maiorov B, Wang H, Wimbush S C, Kursumovic A, Lee J H and MacManus Driscoll J L 2009 Self assembled, rare Earth tantalate pyrochlore nanoparticles for superior flux pinning in $YBa_2Cu_3O_{7-\delta}$ films *Supercond. Sci. Technol.* **22** 022001

[7] Foltyn S R, Civale L, MacManus Driscoll J L, Jia Q X, Maiorov B, Wang H and Maley M 2007 Materials science challenges for high temperature superconducting wire *Nat. Mater.* **6** 631

[8] Haberland H, Mall M, Moseler M, Qian Y, Reiners T and Thurner Y 1994 Filling of micron sized contact holes with copper by energetic cluster impact *J. Vac. Sci. Technol.* A **12** 2925

[9] Stappert S, Rellinghaus B, Acet M and Wassermann E F 2003 Gas phase preparation of L1(0) ordered FePt nanoparticles *J. Cryst. Growth* **252** 440

[10] Sparing M, Backen E, Freudenberg T, Hühne R, Rellinghaus B, Schultz L and Holzapfel B 2007 Artificial pinning centres in YBCO thin films induced by substrate decoration with gas phase prepared Y_2O_3 nanoparticles *Supercond. Sci. Technol.* **20** S239

[11] Hammond R H and Bormann R 1989 Correlation between the *in situ* growth conditions of YBCO thin films and the thermodynamic stability criteria *Physica* C **162** 703

[12] Kwok H S and Ying Q Y 1991 Dynamics of *in situ* $YBa_2Cu_3O_7$ superconducting film formation *Physica* C **177** 122

[13] Gallagher P K, Obryan H M, Sunshine S A and Murphy D W 1987 Oxygen stoichiometry in $Ba_2YCu_3O_x$ *Mater. Res. Bull.* **22** 995

[14] Granqvist C G and Buhrman R A 1976 Ultrafine metal particles *J. Appl. Phys.* **47** 2200

[15] 2015 Database PDF 4+ 2015, International Centre for Diffraction Data: PDF card 00 038 1478 (hexagonal HfO_2); PDF card 00 034 0104 (monoclinic HfO_2) www.icdd.com

[16] Backen E, Hänisch J, Hühne R, Tscharntke K, Engel S, Thersleff T, Schultz L and Holzapfel B 2007 Improved pinning in YBCO based quasi multilayers prepared by on and off axis pulsed laser deposition *IEEE Trans. Appl. Supercond.* **17** 3733

[17] Llordés A *et al* 2012 Nanoscale strain induced pair suppression as a vortex pinning mechanism in high temperature superconductors *Nat. Mater.* **11** 329

[18] Erbe M *et al* 2015 $BaHfO_3$ artificial pinning centres in TFA MOD derived YBCO and GdBCO thin films *Supercond. Sci. Technol.* **28** 114001

[19] Sieger M, Hänisch J, Pahlke P, Sparing M, Gaitzsch U, Iida K, Nast R, Reich E, Schultz L, Holzapfel B and Hühne R 2015 $BaHfO_3$ doped thick $YBa_2Cu_3O_{7-\delta}$ films on highly alloyed textured Ni W tapes *IEEE Trans. Appl. Supercond.* **25** 6602604

[20] Williams D B and Carter C B 2009 *Transmission Electron Microscopy A Textbook for Materials Science* (New York: Springer)

[21] Reich E 2012 *Schichtwachstum und Supraleitung von kupratbasierten Quasimultilagen und Oxipniktiden* (Dresden: TUDpress)

[22] Kiessling A, Hänisch J, Thersleff T, Reich E, Weigand M, Hühne R, Sparing M, Holzapfel B, Durrell J H and Schultz L 2011 Nanocolumns in $YBa_2Cu_3O_{7-x}/BaZrO_3$ quasi multilayers: formation and influence on superconducting properties *Supercond. Sci. Technol.* **24** 055018

[23] Emergo R L S, Wu J Z, Haugan T J and Barnes P N 2005 Tuning porosity of $YBa_2Cu_3O_{7-\delta}$ vicinal films by insertion of Y_2BaCuO_5 nanoparticles *Appl. Phys. Lett.* **87** 232503

[24] Civale L *et al* 2004 Influence of crystalline texture on vortex pinning near the *ab* plane in $YBa_2Cu_3O_7$ thin films and coated conductors *Physica* C **412 414** 976

[25] Pahlke P, Hering M, Sieger M, Lao M, Eisterer M, Usoskin A, Strömer J, Holzapfel B, Schultz L and Hühne R 2015 Thick high J_c YBCO films on ABAD YSZ templates *IEEE Trans. Appl. Supercond.* **25** 6603804

[26] Strickland N M, Long N J, Talantsev E F, Hoefakker P, Xia J A, Rupich M W, Zhang W, Li X, Kodenkandath T and Huang Y 2004 Nanoparticle additions for enhanced flux pinning in YBCO HTS films *Curr. Appl. Phys.* **8** 372

[27] De Keukeleere K *et al* 2016 Superconducting $YBa_2Cu_3O_{7-\delta}$ nanocomposites using preformed ZrO_2 nanocrystals: growth mechanisms and vortex pinning properties *Adv. Electron. Mater.* **2** 1600161